Elsevier Editorial System(tm) for Materials Science & Engineering A
Manuscript Draft

Manuscript Number:

Title: Impact of anisotropy and viscosity to model the mechanical behavior of Ti-6Al-4V alloy

Article Type: Research Paper

Keywords: Elasto-viscoplastic modeling; CPB06 yield criterion; Ti-6Al-4V alloy; plastic anisotropy; strength differential (SD).

Corresponding Author: Mr. Víctor Tuninetti,

Corresponding Author's Institution: University of Liège

First Author: Víctor Tuninetti

Order of Authors: Víctor Tuninetti; Anne-Marie Habraken

Abstract: This paper compares the predictions of an isotropic-thermo-elasto-viscoplastic approach and of an anisotropic-thermo-elastoplastic one with experimental results representative of the mechanical behavior of Ti-6Al-4V at moderate temperatures and low strain rates. The first model is the well known Norton-Hoff viscoplastic constitutive law with isotropic von Mises yield locus identified by using monotonic tension tests performed at strain rates from 10-3 s-1 to 10-1 s-1 and at temperatures up to 400°C. The second model is a thermo-elasto-plastic one defined by the orthotropic yield criterion CPB06. It takes into account the anisotropy and the strength differential (SD) effect in tension-compression of Ti-6Al-4V at RT, 150°C and 400°C. The identification of the SD effect is done by using tension and compression tests and the anisotropy behavior is identified by using shear, plane strain, tension and compression tests performed in three orthogonal material directions. The accuracy of the load and displacements predictions of the two macroscopic constitutive models are compared to experimental results obtained from tests performed on specimens with multiaxial loadings and large strain at several temperatures.

Cover Letter

Université de Liège

Faculté des Sciences Appliquées
Département d'Architecture, Géologie, Environnement et Constructions
Víctor TUNINETTI, PhD. candidate

ArGEnCo

Liège, 21th January 2014

Dear Editor,

Enclosed is a paper, entitled "Impact of anisotropy and viscosity to model the mechanical behavior of Ti-6Al-4V alloy". Please accept it as a candidate for publication in Materials Science and Engineering: A.

The paper compares the predictions of an isotropic-thermo-elasto-viscoplastic approach and of an anisotropic-thermo-elastoplastic one with experimental results representative of the mechanical behavior of Ti-6Al-4V at moderate temperatures and low strain rates. This research paper not only focuses on capturing the experimentally observed tension-compression asymmetry, anisotropy and the strain rate sensitivity of the alloy investigated, but check also that Finite Element simulations with both models can provide accurate load and shape evolution of specimens submitted to multiaxial loading and large plastic strains. These identified material models can be used not only for FE simulations of cold and warm bulk forming processes of TA6V, but also for aircraft structural or engine components design at operating temperatures. The current study helps designers to make the right decision in choosing the constitutive law for the simulations of the mechanical behavior of the TA6V alloy with similar microstructure as the one studied here.

I affirm that all authors have read the paper and agree to the statement of originality of the work. Finally, this paper is our original unpublished work and it has not been submitted to any other journal for reviews.

Please send all the correspondence to the coordinates that appear below.
Best regards,

Víctor Tuninetti.

Département ArGEnCo - Secteur MS²F
Chemin des chevreuils, 1 BAT. B52/3 +1 B-4000 Liège 1 (Belgique)
Tél. ++ 32 (04) 366 92 19 Fax. ++ 32 (04) 366 91 92 Parking P52
Email: V.Tuninetti@ulg.ac.be www.argenco.ulg.ac.be/MS²F

Impact of anisotropy and viscosity to model the mechanical behavior of Ti-6Al-4V alloy

V. Tuninetti[1*], A.M. Habraken[1,2]

[1] ARGENCO Department, MS[2]F Division, University of Liège,
Chemin des Chevreuils 1, 4000 Liège, Belgium

[2] Research Director of the Fonds de la Recherche Scientifique - FNRS, Belgium

Keywords: Elasto-viscoplastic modeling; CPB06 yield criterion; Ti-6Al-4V alloy; plastic anisotropy; strength differential (SD).

Abstract: This paper compares the predictions of an isotropic-thermo-elasto-viscoplastic approach and of an anisotropic-thermo-elastoplastic one with experimental results representative of the mechanical behavior of Ti-6Al-4V at moderate temperatures and low strain rates. The first model is the well known Norton-Hoff viscoplastic constitutive law with isotropic von Mises yield locus identified by using monotonic tension tests performed at strain rates from 10^{-3} s^{-1} to 10^{-1} s^{-1} and at temperatures up to 400°C. The second model is a thermo-elasto-plastic one defined by the orthotropic yield criterion CPB06. It takes into account the anisotropy and the strength differential (SD) effect in tension-compression of Ti-6Al-4V at RT, 150°C and 400°C. The identification of the SD effect is done by using tension and compression tests and the anisotropy behavior is identified by using shear, plane strain, tension and compression tests performed in three orthogonal material directions. The accuracy of the load and displacements predictions of the two macroscopic constitutive models are compared to experimental results obtained from tests performed on specimens with multiaxial loadings and large strain at several temperatures.

1. Introduction

Over the last few years, numerous experimental studies have been carried out on Ti-6Al-4V (called hereafter TA6V) alloy in order to characterize its mechanical behavior as a function of strain rates and temperature. The reported results in the literature [1, 2, 3, 4, 5, 6, 7, 8, 9, 10, 11] show that the yield stress of this two phase α+β-type alloy is strongly dependent on both temperature and strain rate. Like many other metals, the higher the strain rate, the greater is the yield stress. On the other hand, the stress level decreases when temperature increases. Nevertheless, the effect of the temperature on the yield stress has been found greater than the one of the strain rate for low and high strain rates and temperatures from RT to 1000K [3,4]. Both Lee and Lin [3] and Arrieta and Espinosa [12], explain that the increase of temperature tends to reduce the yield stress by lowering the thermally activated part of the resistance to dislocation motions.
There are many different constitutive models currently available to describe the strain hardening, strain-rate hardening, and thermal softening of materials with specific material constants. Two categories can be distinguished. In the first one, there are the physically based models, which consist in models based on the deformation mechanism

* Corresponding author: V.Tuninetti@ulg.ac.be; tel.: +32 43669219; fax: +32 43669534.

at the scale level of dislocations, e.g., Mechanical Threshold Strength (MTS) model [13], Zerilli-Armstrong (Za) model [14], etc. In the second category, there are the purely phenomenological models, e.g., Johnson-Cook (JC) [15], Norton-Hoff (NH) [16] and Khan-Huang-Liang (KHL) [4] models, etc. Most of the studies available in the literature [17, 18, 4, 5, 19, 6, 11] focus on capturing softening, workability, work hardening for cold (RT), warm (around 400°C) and hot working processes (around 900°C). The validation of these models is essentially based on predictions of the true stress-strain curves of experimental tests.

In addition to strain rate and temperature dependence, experimental results published by several researchers [19, 6, 20, 21, 22, 23] show that TA6V also exhibits a strength differential (SD) effect, and a distortion of the yield surface with the accumulated plastic deformation. Nixon et al. [24] and Gilles et al. [21] explain that SD effect is the result from the combination of a sharp initial basal texture and the polarity of deformation twinning, even for monotonic loadings. Furthermore, Plunkett et al. [25] explains that because of twinning and texture evolution, the yield surface for hexagonal close-packed (hcp) metals significantly changes shape with the accumulated plastic deformation. The above mentioned anisotropic features are captured for instance by the macroscopic orthotropic yield criterion CPB06 proposed by Cazacu et al. [26].

Many commercial FE codes offer isotropic viscoplastic and anisotropic elastoplastic constitutive models to describe material behavior. However, even if some authors propose anisotropic viscoplastic approach (Bron and Besson [27], Plunkett et al. [28]) the standard user of commercial codes in industry has generally to choose between neglecting viscosity or anisotropy. For this reason, the current study presents an evaluation of the mechanical modeling of TA6V alloy by comparing the prediction accuracy of these two types of macroscopic plasticity models. The first one is the Norton-Hoff constitutive law with the isotropic von Mises yield locus which accounts for isotropic-thermo-viscoplastic behavior of materials and the second one is the CPB06 yield criterion modeling the plastic anisotropy and the SD effect. In both cases, elasticity follows Hooke's law taking into account anisotropic elastic coefficients.

The identification of the Norton-Hoff (NH) constitutive model is based on tension tests performed in one material direction at constant strain rates equal to 10^{-3}, 10^{-2} and 10^{-1} s^{-1} and at room temperature (RT), 150°C and 400°C for a forged TA6V alloy. A study of temperature and strain rate sensitivity of the plastic behavior of the alloy is also presented hereafter.

The identification of the CPB06 yield loci for the same TA6V has already been described in Tuninetti et al. [29] at RT and at one strain rate equal to 10^{-3} s^{-1}. In addition, a new set of parameters of CPB06 identified at 150°C and 400°C is computed in this study, using tension and compression tests performed at a constant strain rate equal to 10^{-3} s^{-1} and at 150°C and 400°C.

In the current paper, the capacities of the two identified models (CPB06 and NH) to accurately reproduce the plastic behavior of TA6V at several temperatures and low strain rate range are evaluated. The error between FE predictions and experimental data allows quantitative comparison of the accuracy of the two models in force and displacement predictions on specimens subjected to multiaxial tensile and compressive loading, with different initial stress triaxialities and large strains. The tests used for the models validation are compression tests on elliptical cross-section specimens, tensile tests on notched round bars and tensile tests on holed round bars performed at

temperatures up to 400°C. Note that none of these tests were included in the database used for the identification of the models.
These identified material models can be used not only for FE simulations of cold and warm bulk forming processes of TA6V, but also for aircraft structural or engine components design at operating temperatures. The current study helps designers to make the right decision in choosing the constitutive law for the simulations of the mechanical behavior of the TA6V alloy with similar microstructure as the one studied here.
This paper is organized as follows:

- Section 2 describes the experimental framework used to perform the tests and the features of the alloy investigated.
- Section 3 presents the experimental results obtained: elastic parameters, strain rate and temperature sensitivity as well as tension-compression asymmetry or strength differential (SD) effect.
- Section 4, introduces the Norton-Hoff and the CPB06 models identified in this paper. Then, it presents the comparisons of their analytical predictions with experimental uniaxial stress-strain curves used for their identification.
- Section 5 focuses on the evaluation of the predictions of the models.
- Finally, in section 6 the overall conclusions are highlighted.

Note that damage is not addressed in this paper. As verified, it does not prevent the constitutive laws to model the TA6V behavior even for large plastic strain after the onset of necking. This fact is related to the mechanism of ductile fracture in TA6V due to void nucleation, growth and coalescence which is strongly localized and affects the mechanical behavior only for states very close to rupture [30, 31].

2. Material properties, testing equipments and experimental procedures

2.1. Material

TA6V is a α-β-type alloy with β transus temperature of about 996°C. The aluminum alloying element stabilizes the α (hcp) phase, i.e., it increases the temperature at which this α phase is stable. On the other hand, vanadium alloying is β (bcc) stabilizer which results in stability of the β phase at lower temperatures [32]. The bulk forged TA6V alloy investigated in this study has a chemical composition given in Table 1. The three orthogonal directions of the material are named here after as LD, TD and ST (Fig. 1). The hcp α-phase represents 94% of the volume. Optical microscopy showed that the material has slightly elliptic grain and that the mean grain size is equal to 12 µm in the ST-LD plane and 9µm in ST-TD plane [30].

2.2. Monotonic compression and tensile tests at several temperatures and strain rates

The compression tests performed at RT are conducted using a servohydraulic testing machine which is controlled in order to impose constant strain rates equal to 10^{-3}, 10^{-2}, and 10^{-1} s^{-1}. For the tests at elevated temperatures (between 150°C and 800°C) the testing machine is equipped with an Infrared (IR) furnace (Quad Ellipse Chamber, Model E4, Radiant Energy Research Inc.) and the targeted constant strain rate is equal

to 10^{-3} s^{-1}. Stress-strain curves for compression tests are computed by using the method proposed by Tuninetti et al. [33].
The tensile tests are performed at constant strain rates equal to 10^{-3}, 10^{-2}, and 10^{-1} s^{-1} for each level of temperature (RT, 150°C and 400°C). A universal testing machine (electro-mechanic Press ZWICK 100 kN) equipped with a furnace (fours H&C S.P.R.L) with three independent heating zones is used.
Prior to both tensile and compression tests, the specimens were held for 5 minutes at the testing temperature in order to ensure a homogeneous temperature distribution through the specimens. The experimental setup at elevated temperatures did not allow the use of an extensometer or optical measurements. For this reason, a procedure for the correction of the deflection of testing machine was developed and implemented in order to reach constant strain rates. All of the monotonic compression and tensile tests are performed in the longitudinal material direction (LD) for all the investigated temperatures and strain rates. The anisotropy was investigated by means of other tests not described here. The interested reader can refer the work of Tuninetti et al. [29].

3. Tensile and compression experimental results

Table 2 shows the average initial yield strength and the Young's modulus with the standard deviation. The experimental material data show that the alloy involves strain rate and temperature sensitive properties, as well as SD effect.

3.1. Strain rate sensitivity

The tensile yield stress as a function of the strain rate at 0.02 of true plastic axial strain in tensile tests is presented in Fig. 2. The usual value of 0.2% of plastic strain to define yield stress is not adopted because it is not representative of the studied plastic range. A linear increase of the yield stress with the strain rate is observed at RT and 150°C, and a weak strain rate influence on the yield stress is found at 400°C.

3.2. Temperature sensitivity

Fig. 3 shows the evolution of the yield stress at 0.02 of true plastic strain with the temperature under several low strain rates. A strong effect of the temperature on the yield stress is observed. The stress rapidly decreases with the increase of the temperature for all the investigated strain rates. Note that at low strain rates ($<10^{-1}$ s^{-1}) the temperature increase on the sample associated to plastic work is negligible and therefore the tests are considered as isothermals.

3.3. SD effect and anisotropic hardening

Tensile and compression true stress/strain curves of test performed at constant strain rate equal to 10^{-3} s^{-1} are shown in Fig. 4(a). These curves demonstrate that the hardening rate is different in tension and in compression and varies with the temperature. Fig. 4(b) gathers the values of yield stress evolution with the temperature for tension and compression at a true strain value equal to 0.02. Based on this experimental information,

it can be concluded that the material response of TA6V demonstrates a strength asymmetry between tension and compression (SD effect) for the temperature range investigated but a weak asymmetry at 400°C.

4. Mathematical modeling

In this section, the Norton-Hoff and the CPB06 models and their identification methods are presented. In addition, the comparisons of their analytical predictions with experimental results are reported.

4.1. Identification of the elasto-thermo-viscoplastic Norton-Hoff model

A non-linear thermo-viscoplastic formulation with the strain rate sensitivity introduced by the Norton-Hoff material model is chosen to predict the observed dependence of the yield stress on the strain, strain rate and temperature of TA6V at large strains. The Norton-Hoff (NH) law was introduced by Norton [16] in order to describe the uniaxial creep of steel at high temperature and extended by Hoff [34] to the multiaxial loadings. The constitutive equation is defined as follows:

$$\bar{\sigma} = \exp(-P_1\bar{\varepsilon})\sqrt{3}P_2(\sqrt{3}\dot{\bar{\varepsilon}})^{P_3}\,\bar{\varepsilon}^{P_4} \tag{1}$$

where $\bar{\sigma}$ is the equivalent stress, $\bar{\varepsilon}$ the equivalent total strain and $\dot{\bar{\varepsilon}}$ the equivalent strain rate. The material parameters P_1, P_2, P_3 and P_4 are respectively related to softening, strength, viscosity and hardening behaviors and they are all thermally affected. The equivalent stress is associated to the von Mises yield criterion and the viscoplastic strain tensor $\dot{\boldsymbol{\varepsilon}}^{vp}$ as a function of stress tensor $\boldsymbol{\sigma}$ is given by [35]:

$$\dot{\boldsymbol{\varepsilon}}^{vp} = \frac{J_2^{P_5}\exp\left(\dfrac{P_1}{P_3}\bar{\varepsilon}\right)\bar{\varepsilon}^{-\frac{P_4}{P_3}}}{2\left(P_2\right)^{\frac{1}{P_3}}}\boldsymbol{\sigma} \tag{2}$$

where $J_2 = \dfrac{1}{3}\bar{\sigma}^2$ and $P_5 = \dfrac{1-P_3}{2P_3}$

The set of NH model parameters is identified at three levels of temperatures, RT, 150 and 400°C by using the experimental equivalent tensile strain-stress curves at strain rates equal to 10^{-3}, 10^{-2} and 10^{-1} s^{-1} (LD direction). A direct identification method is chosen which uses the Nelder-Mead Simplex algorithm [36]. P_1, P_2, P_3 and P_4 are obtained by minimizing the weighted mean square error (*MSE*) between the experimental (*Exp*) and the model (*NH*) stress-strain curves defined as:

$$MSE = \sum_{\dot{\varepsilon}}\sum_{\bar{\varepsilon}} w_{\dot{\varepsilon}}\left(\frac{\bar{\sigma}^{Exp}\left(\dot{\bar{\varepsilon}},\bar{\varepsilon}\right) - \bar{\sigma}^{NH}\left(\dot{\bar{\varepsilon}},\bar{\varepsilon}\right)}{\bar{\sigma}^{Exp}\left(\dot{\bar{\varepsilon}},\bar{\varepsilon}\right)}\right)^2 \tag{3}$$

The identified NH parameters are given in Table 3 and their evolutions are shown in Fig. 5. The effect of softening does not appear in the investigated domain of temperatures

and plastic strain and P_1 is set with a zero value. The tensile curves were used only until the ultimate stress level (at strains between 0.8 and 0.1 depending on strain rate and temperature) as Digital Image Correlation technique was not used for all the uniaxial tensile tests preventing to have access to true stress-strain curves. The lack of softening as well as of damage within the models is the general case for many users who either cannot identify them in an accurate way or have no access to complex laws. One can check in section 5 that these strong assumptions do not yield to a strong lost of accuracy for the TA6V studied.
As already observed in the experimental results section 3, the increase of temperature decreases the parameter P_2 related to the strength of the material (Fig. 5(a)). The strain rate sensitivity parameter P_3 increases from RT to 150°C and becomes negligible at 400°C, which indicates that for this latter temperature no strain rate effect occurs (Fig. 5(b)). The evolution of P_4 with the temperature shown in Fig. 5(c) demonstrates that hardening gradually increases with rising temperature.
An overview of the NH model predictions of true stress–strain curves in tensile (used for the identification) and compression (not used for identification) states compared with experiments is shown in Figs. 6-7. The model properly describes the initial yield stress and strain hardening of the TA6V for the three investigated strain rates and temperatures in uniaxial tensile (Fig. 6), but this is not the case in the uniaxial compression (Fig. 7). These results are the expected ones as the NH model takes into account neither SD effect nor anisotropic hardening.

4.2. Identification of the orthotropic CPB06 yield criterion

The orthotropic yield criterion CPB06 was developed by Cazacu et al. [26]. The criterion is defined by:

$$F_1 = \left(|\Sigma_1| - k\,\Sigma_1\right)^a + \left(|\Sigma_2| - k\,\Sigma_2\right)^a + \left(|\Sigma_3| - k\,\Sigma_3\right)^a \tag{4}$$

k is a parameter which takes into account the strength differential effect (SD) and a is the degree of homogeneity. $\Sigma_1, \Sigma_2, \Sigma_3$ are the principal values of the tensor $\boldsymbol{\Sigma}$ defined by $\boldsymbol{\Sigma} = \mathbf{C} : \mathbf{S}$ where $\mathbf{C}$ is a fourth-order orthotropic tensor that accounts for the plastic anisotropy of the material and $\mathbf{S}$ is the deviator of the Cauchy stress tensor.
Tuninetti et al. [29] uses directional hardening that takes into account of the distortion of the yield locus. The anisotropy coefficients C_{ij} and the SD parameter k are obtained for five fixed levels of plastic work and then the model uses a piece-wise linear interpolation to obtain the yield surface corresponding to any level of plastic work. The updated yield locus is described by

$$f\left(\boldsymbol{\sigma}, \bar{\varepsilon}_p\right) = \bar{\sigma}\left(\boldsymbol{\sigma}, \bar{\varepsilon}_p\right) - Y\left(\bar{\varepsilon}_p\right) \tag{5}$$

$\bar{\sigma}$ is the equivalent plastic stress associated to the given yield criterion in Eq. (4) while $\bar{\varepsilon}_p$ is the equivalent plastic strain associated to $\bar{\sigma}$ using the work-equivalence principle [37] and $Y\left(\bar{\varepsilon}_p\right)$ is a reference hardening curve defined as:
$Y\left(\bar{\varepsilon}_p\right) = A_0 + B_0\left[1 - \exp\left(-C_0\bar{\varepsilon}_p\right)\right]$ where A_0, B_0, C_0 are material constants. For any $\bar{\varepsilon}_p$, the plastic work per unit volume is given by:

$$W_p\left(\bar{\varepsilon}_p\right)=\int_0^{\bar{\varepsilon}_p} Y(p)dp=(A_0+B_0)\bar{\varepsilon}_p-\frac{B_0}{C_0}\left(1-\exp\left(-C_0\bar{\varepsilon}_p\right)\right) \quad (6)$$

The anisotropy coefficients and SD parameters evolve as a function of the plastic work per unit volume W_p. This methodology was first proposed by Plunkett et al. [25] by considering accumulated plastic strain and further adapted by Gilles et al. [21] by considering plastic work levels.

Tuninetti et al. [29] identified continuous yield surfaces of CPB06 at five plastic work levels in three orthogonal directions of the material at RT and at 10^{-3} s^{-1} for the same bulk TA6V alloy investigated in the present study. The identification was based on a set of monotonic tests: uniaxial tensile, uniaxial compression, simple shear and plane strain and an inverse modeling of strain fields measured by DIC in compression specimens was used. The excellent capabilities of the model were validated not only in the set of monotonic stress-strain curves but also in specimens (notched tensile tests) with multiaxial loading with accurate results.

The anisotropy coefficients and SD parameters of CPB06 yield criterion at RT obtained by Tuninetti et al. [29] are used in this paper (Table 4-5).

In order to predict the SD effect and anisotropy of TA6V at higher temperatures, the CPB06 model is identified in the present study at 150°C and 400°C and at 10^{-3} s^{-1} using only tension and compression tests in LD direction (Table 4-5). The anisotropy coefficients C_{ij} are kept constant, but k coefficients and hardening are temperature dependent. This assumption appears quite strong as microstructure events such as different twining activities and texture evolution with temperature could be expected. However, validation section confirms that the possible loss of accuracy model predictions due to this assumption can be neglected.

The five levels of plastic work considered for each set of parameters are computed at the same amount of equivalent plastic strain as the ones used for RT. A_0, B_0, C_0 are obtained by fitting the reference hardening curves $Y\left(\bar{\varepsilon}_p\right)=A_0+B_0\left[1-\exp\left(-C_0\bar{\varepsilon}_p\right)\right]$ with the tensile tests at each identification temperature. SD parameters (k) are computed for each plastic work level by fitting the experimental and numerical yield stress ratios between tension and compression using the Simulated Annealing (SA) algorithm [38, 39].

The biaxial plane projections of the identified CPB06 yield loci (lines) in LD-TD at RT, 150°C and 400°C and at 10^{-3} s^{-1} along with the experimental values (symbols) for the five levels of plastic work are shown in Fig. 8. Correlations demonstrate that the CPB06 law predicts the distortion of the yield surface with the variation of plastic work and also the asymmetry between tension and compression for all the range of temperatures.

5. Assessment of predictions of the thermo-viscoplastic Norton-Hoff model and the orthotropic yield criterion CPB06 versus experimental results.

Compression tests on elliptical cross-section specimens and tensile tests on holed and V-notch specimens with geometries presented in Fig. 9 are tested and compared with FE simulations in order to evaluate the two identified models.

One-eighth of the specimens is meshed. The updated Lagrangian FE code Lagamine is chosen and the thermomechanical mixed solid finite element BLZ3T [40] is used for

simulation with the Norton Hoff constitutive law. The latter is based on an implicit integration scheme [41]. BWD3D finite element is used for the simulations with CPB06 law. Both finite elements are 8-node 3D brick elements with a mixed formulation adapted to large strains and large displacements. They use a reduced integration scheme (with only one integration point) and an hourglass control technique. These elements are based on the non-linear three-field (stress, strain and displacement) HU-WASHIZU variational principle [42, 43, 44].
The experimental and predicted axial load and displacement curves are used to assess the predictions of the models.

5.1. Mesh sensitivity analysis

In order to verify the accuracy of the FE simulations with the identified constitutive laws, the NH and the CPB06 simulations are applied on a tensile test on a V-notch round bar. A sensitivity evaluation to the mesh density of the predicted cross-sectional areas just before experimental fracture is performed. This geometry is chosen as it presents stress concentration at the sharp edge. Four meshes are used with a progressive increase in the number of elements along the three orthogonal directions of the sample (see Fig. 10(a)). The results show a low influence of the mesh density on the computation of the cross-sectional area (Fig. 10(b)). This low sensitivity was expected, as the global variation of the plastic behavior of the entire cross-section with the mesh density is affected by a very localized variation of the behavior on the sharp edge. Despite this low sensitivity, the measured cross-sectional area is found a little higher than the predicted ones. Similar phenomenon in tensile tests on U-notch round bar is presented in Tuninetti et al. [29]. It could be partially explained by the volume conservation and dense matrix assumptions used in the chosen plasticity models which neglect of the porosity of the material. The void volume fraction of 0.57% is present in the material just before fracture in a uniaxial tensile test [30] when error of volume of 0.75% is computed in the cross-section. Another reason could be also related to a necking event predicted too early. For each model, a different reason could be responsible: isotropic-visco-plastic NH model presents a too low strength because it neglects anisotropy behavior (see Fig. 13), when the natural regularization brought by viscosity and delaying necking is missing in elastoplastic Cazacu model. Finally, a fine mesh density (18 elements along the radius of the minimal cross-section of the V-notch round bar) is chosen as a compromise between good numerical accuracy and CPU time efficiency of the simulations.

5.2. Load predictions

5.2.1. Tensile tests

The tensile tests are performed on the two geometries shown in Fig. 9(b) until fracture at RT, 150°C and 400°C. Figs. 11-12 show the evolution of the load with the axial displacement of a gauge length of the specimen equal to 40mm for the tests performed at RT and 60 mm for the tests at 150°C and 400°C. The experimental curves are presented as the average of three tests with the respective error bars. The large error bars represent the tensile fracture zone. The linear elastic increment of the load with the axial displacement is well predicted for all the simulations. Such a result allows validating the

Young's modulus indentified at several temperatures in LD direction by using simple tensile tests.

Eq. 7 is used in order to quantify the accuracy of the load predictions $\left(F^{\text{model}}\right)$ of both models compared with experimental data $\left(F^{\text{exp}}\right)$ at several fixed values of axial displacements (*i*) equal to multiples of 0.2mm (*m* is the total number of values used in each curve).

$$\text{Error} = \frac{1}{m}\sum_{i=1}^{m}\frac{\left|F_i^{\text{exp}} - F_i^{\text{model}}\right|}{F_i^{\text{exp}}} \tag{7}$$

The axial load predictions in the plastic zone for the V-notch round bars shown in Fig. 11 are overestimated by the NH model at the three temperatures suggesting a too high hardening extrapolated curve. Better load correlations are obtained from simulations using CPB06 model with an error lower than 3.6% at RT and 150°C. The CPB06 predictions are very accurate at 400°C with an error equal to 1.2%. It should be considered that the CPB06 model identification is different at RT than the ones at 150°C and 400°C. The latter were performed with only tensile and compression tests in one direction of the material, while the CPB06 yield criterion at RT was identified with stress-strain data in the three orthogonal directions of the material for tensile and compression tests and in one direction for simple shear and plane strain tests (Fig. 13). Even though error predictions by CPB06 are low, they could still be reduced to smaller values. The errors at the beginning of the plastic zone are attributed to the purely empirical bases of the material models and the fact that the stress state in the V-notch is far from the stress states included in the identification of the models.

The axial load predictions from the tensile test of round bars with a central hole by the two models are more accurate than the ones for V-notch for all the temperature range investigated (Fig. 12). This could be attributed to the closer stress state in the specimen to uniaxial stress state used in the identification of both models. However, a slight decrease of the predicted load before fracture found with both models does not represent the feature experimentally observed. This effect could be attributed to the identification of the strain hardening law (NH) and yield surfaces (CPB06) which are performed with true stress-strain curves till strain value equal to 0.1 (before the onset of necking in simple tensile tests), and the fact that the strain reached in the minimal cross-section of the specimen with central hole is much higher (maximum strain value equal to 0.33), so the real hardening after the axial strain equal to 0.1 is unknown and assumed to follow the constitutive hardening law of the model.

For the last part of the experimental load-displacement curves, the sudden decrease of the experimental load is attributed to a damage of the material which is not taken into account by the studied models.

As a conclusion, the gap between the experimental results and the simulations in tensile tests with V-notch and central hole at RT and 150°C could be explained by the fact that the stress states in the V-notch and O-holed are far from the ones used in the identification of the constitutive laws, specially for V-notch. Inverse modeling for instance could be applied to improve the prediction. Also, it can be seen from Fig. 13 that the initial shear yield stress was overestimated in the identification of both CPB06 and NH models at RT. This overestimation increases the axial load in notch round bars

where higher shear stress takes place. However, the maximum error on the load prediction with CPB06 is low (around 3% for round bar with central hole and less than 3.6% for V-notch).

5.2.2. Compression tests

The compression tests are performed on specimens shown in Fig. 9(a) until 16% of average axial strain. These tests are performed at three different strain rates (10^{-3}, 10^{-2} and 10^{-1} s^{-1}) for RT and at one strain rate equal to 10^{-3} s^{-1} for 150°C and 400°C. Fig. 14(a) shows the axial load versus axial displacement of the compression specimens with elliptical cross-sections and Fig. 14(b) assesses simulation results versus experiments. The variation of the compressive load with the strain rate is not well predicted by NH model, nor of course by the CPB06 model (Fig. 14(a)). Even though NH takes into account the strain rate sensitivity of TA6V, the predicted load with this model is much lower than the ones obtained by the experiments, and the one obtained with the CPB06 model. The latter model provides a more accurate load computation insensitive to strain rate than the NH model (Fig. 14b, Eq. 7). This can be explained by the fact that the tension-compression strength asymmetry observed in the TA6V is only taken into account by the CPB06 model. The same conclusion is obtained from the observation between the predicted and experimental compressive loads on tests at several temperatures (Fig. 14(d)), where CPB06 presents a high accuracy load prediction (Fig. 14(e)).

5.3. Shape predictions

5.3.1. O-Holed bar tensile test

The use of 3D-DIC allows measuring the entire experimental strain and displacement fields of the tested samples with accurate results. Fig. 15 shows the evolution of the true axial strain field and geometry measured on the tensile round bar with a central hole at RT. The predictions of the evolution of necking (diameter D, Fig. 16(b)) with the experimental value until fracture are compared in Fig. 16(a). NH model largely underestimates the value of D when the anisotropic CPB06 model shows closer predictions to the experimental values in the entire loading range.

5.3.2. Compression test

The compression tests performed at 10^{-3} s^{-1} and at RT is also used to assess the shape predictions of the models. The evolution of the lengths of the minor (2b) and major (2a) axes of the elliptical cross-section of the specimens are shown in Fig. 17. Both models closely predict the major axis length but the viscoplastic Norton-Hoff results neglecting anisotropy differ more and more from the experimental value of the minor axis length with the increase of the loading. The latter isotropic model cannot simulate the true anisotropic plastic flow.

6. Conclusions and perspectives

The mechanical response of TA6V was studied with a set of tension and compression tests performed at moderate temperatures up to 400°C and a range of strain rates between 10^{-3} and 10^{-1} s^{-1}. Mechanical properties such as yield stress, strain hardening, strain rate hardening, strength differential effect and their evolution with the temperature were determined. The influence of the temperature on these properties was found being higher than the one of the strain rate. Furthermore, the experimental data were used for the identification of the material parameters of CPB06 and Norton-Hoff constitutive laws at RT, 150°C and 400°C.
The followings points are the main findings regarding the assessment of both models to predict the load and displacements on specimens with several initial stress triaxialities:

- NH model accurately fits the experimental strain and strain rate hardening of monotonic tests TA6V only for the type of loading and material direction used for its identification (in this case, uniaxial tensile in LD direction). This is due to the fact that the model takes into account neither the SD effect nor the anisotropic behavior of the alloy.
- The CPB06 model results show a better experimental correlation than the NH model predictions, for all the range of temperatures investigated. It is attributed to the ability of the model to capture the SD effect and distortion of the anisotropic yield surface of the TA6V. However, this model does not take into account the change of yield surface with the strain rate. Its accuracy is limited to the strain rate range chosen for its identification and depends on the strain rate sensitivity of the alloy.
- The maximum and global average Error values in load prediction on all the validation tensile tests were found to be equal to 3.6% and 2.0 % for the CPB06 model, while for the NH model, these errors were equal to 10.4% and 5.6%.
- The shape of the specimens used for the validation tests at RT were also compared with the predictions of the plasticity models:
    - In compression tests on elliptical cross-section specimens, the CPB06 model predicts more accurately the evolution of the shape with a maximum deviation of displacements equal to 0.1 mm in the minor axis length compared to 0.2 mm for the one obtained with the NH model.
    - In the tensile test of round bars with a central hole, good correlations of the evolution of the necking were obtained with the CPB06 model with a maximum deviation of 0.015mm compared to 0.05mm obtained with the NH model.

Finally, based on the extensive experimental and numerical analysis, one concludes that the CPB06 model proposed by Cazacu et al. [26] shows a good and higher accuracy when predicting shape and load on complex specimens of TA6V (several initial triaxilities with axial and radial load, e.g. V-notch, central holed round bars, compression with barreling, etc) than the Norton-Hoff law. If one has no access to an elasto-visco-plastic anisotropic model, it seems better to neglect viscosity than anisotropy for low strain rates.
Furthermore, it is believed that damage models, which take into account the porosity of materials, should be considered in order to improve even more not only the predictions of shape but also of load and fracture of TA6V components.

Acknowledgments

The authors thank the Walloon Region, the Belgian Scientific Research Fund FNRS which finances A.M.H. and the Interuniversity Attraction Poles Program, P7/21 Intemate initiated by the Belgian Science Policy office, for financial support. The authors would also like to thank O. Milis (ULg) for his technical support and assistance.

References

[1] M. Burkins, J. Hansen, J. Paige, P. Turner, The effect of thermomechanical processing on the ballistic limit velocity of extra low interstitial titanium alloy Ti–6Al–4V, U.S. Army research laboratory ARL-MR-486 (2000) 1-69.

[2] M. Burkins, M. Wells, J. Fanning, B. Roopchand, The Mechanical and Ballistic Properties of an Electron Beam Single Melt of Ti-6Al-4V Plate, U.S. Army Research Laboratory, ARL-MR-515 (2001).

[3] W.S. Lee, C.F. Lin, Plastic deformation and fracture behaviour of TA6V alloy loaded with high strain rate under various temperatures, Mater. Sci. Eng. A 241 (1998) 48-59.

[4] A.S. Khan, Y.S. Suh, R. Kazmi, Quasi-static and dynamic loading responses and constitutive modeling of titanium alloys, Int. J. Plasticity 20 (2004) 2233–2248.

[5] A.S. Khan, R. Kazmi, B. Farroch, Multiaxial and non-proportional loading responses, anisotropy and modeling of Ti-6Al-4V titanium alloy over wide ranges of strain rates and temperatures, Int. J. Plasticity 23 (2007) 931–950,

[6] A.S. Khan, S. Yu, H. Liu, Deformation induced anisotropic responses of Ti–6Al–4V alloy Part II: A strain rate and temperature dependent anisotropic yield criterion, Int. J. Plasticity 38 (2012b) 14-26.

[7] A. Majorell, S. Srivatsa, R.C. Picu. Mechanical behavior of TA6V at high and moderate temperatures – Part I: Experimental results, Mater. Sci. Eng. A 326 (2002) 297-305.

[8] J. Peirs, P. Verleysen, J. Degrieck, F. Coghe, The use of hat-shaped specimens to study the high strain rate shear behaviour of Ti-6Al 4V, Int. J. Impact Eng. 37 (2010) 703–714.

[9] H. Meyer Jr., D. Kleponis, Modeling the high strain rate behavior of titanium undergoing ballistic impact and penetration, Int. J. Impact Eng. 26 (2001) 509-52.

[10] A.S. Milani, W. Dabboussi, J.A. Nemes, R.C. Abeyaratne, An improved multi-objective identification of Johnson–Cook material parameters, Int. J. Impact Eng. 36 (2009) 294-302.

[11] S. Seo, O. Min, H. Yang, Constitutive equation for Ti–6Al–4V at high temperatures measured using the SHPB technique, Int. J. Impact Eng. 31 (2005) 735-754.

[12] H.V. Arrieta, H.D. Espinosa, The role of thermal activation on dynamic stress-induced inelasticity and damage in Ti–6Al–4V, Mechanics of Materials 33 (2001) 573-591.

[13] P.S. Follansbee, U.F. Kocks, A constitutive description of the deformation of copper based on the use of the mechanical threshold, Acta Metallurgica 36 (1988) 81–93.

[14] F.J. Zerilli, R.W. Armstrong, Dislocation-mechanics-based constitutive relations for material dynamics calculations, Journal of Applied Physics 61 (1987) 1816–1825.

[15] G.R. Johnson, W.H. Cook, A constitutive model and data for metals subjected to large strains, high strain rates and high temperatures, Proc. of the 7th International Symposium on Ballistics (1983) 541–547.

[16] F. H. Norton, The Creep of Steel at Hight Temperature, The McGraw-Hill, New York, 1929.

[17] C. Zhang, X.q. Li, , D.s. Li, C.h. Jin, J.j. Xiao, Modelization and comparison of Norton-Hoff and Arrhenius constitutive laws to predict hot tensile behavior of Ti−6Al−4V alloy, Trans. Nonferrous Met. Soc. China 22 (2012) s457−s464.

[18] W.S. Lee, M.T. Lin. The effects of strain rate and temperature on the compressive deformation behaviour of Ti-6A1-4V alloy, J. Materials Processing Technology 71 (1997) 235-246.

[19] A.S. Khan, S. Yu, Deformation induced anisotropic responses of Ti–6Al–4V alloy. Part I: Experiments, Int. J. Plasticity 38 (2012a) 1-13.

[20] W. Hammami, W. Tirry, F. Coghe, L. Duchene, L. Delannay, A.M. Habraken, Ti6A14V anisotropy and texture evolution predictions using Multisite and self consistent crystal plasticity models, The 12th World Conference on Titanium Ti-2011 (2011).

[21] G. Gilles, W. Hammami, V. Libertiaux, O. Cazacu, J.H. Yoon, T. Kuwabara, A.M. Habraken, L. Duchêne, Experimental characterization and elasto-plastic modeling of the quasi-static mechanical response of TA–6 V at room temperature, Int. J. Solids Struct. 48 (2011) 1277–1289.

[22] V. Tuninetti, G. Gilles, O. Milis, L. Lecarme, A.M. Habraken, Compression test for plastic anisotropy characterization using optical full-field displacement measurement technique, Steel Res. Int. SE: 14th Int. Conf. Metal Forming 2012 (2012b) 1239-1242.

[23] E.L. Odenberger, J. Hertzman, P. Thilderkvist, M. Merklein, A. Kuppert, T. Stöhr, J. Lechler, M. Oldenburg, Thermo-mechanical sheet metal forming of aero engine

components in Ti-6Al-4V – PART 1: Material characterization, Int. J. Mater. Form. (2012) 1-12.

[24] M.E. Nixon, O. Cazacu, R.A. Lebensohn, Anisotropic response of high-purity α-titanium: experimental characterization and constitutive modeling, Int. J. Plasticity 26 (2010) 516-532.

[25] B. Plunkett, R.A. Lebensohn, O. Cazacu, F. Barlat, Anisotropic yield function of hexagonal materials taking into account texture development and anisotropic hardening. Acta Mater. 54 (2006) 4159-4169.

[26] O. Cazacu, B. Plunkett, F. Barlat, Orthotropic yield criterion for hexagonal close packed metals, Int. J. Plasticity 22 (2006) 1171-1194.

[27] F. Bron, J. Besson, A yield function for anisotropic materials. Application to aluminium alloys, Int. J. Plasticity 20 (2004) 937–963.

[28] B. Plunkett, O. Cazacu, R.A. Lebensohn, F. Barlat, Elastic-viscoplastic anisotropic modeling of textured metals and validation using the Taylor cylinder impact test, I. J. Plasticity 23 (2007) 1001-1021.

[29] V. Tuninetti, G. Gilles, O. Milis, T. Pardoen, A.M. Habraken, Anisotropy and tension-compression asymmetry predictions of the plastic response of bulk Ti-6Al-4V alloy at room temperature, (unpublished results).

[30] L. Lecarme, Viscoplasticity damage and fracture of Ti-6Al-4V, PhD thesis. Université catholique de Louvain, Louvain, 2013.

[31] J. Peirs, Experimental characterisation and modelling of the dynamic behaviour of the titanium alloy Ti6Al4V, PhD thesis, Ghent University, Ghent, 2012.

[32] M.J. Donachie Jr., Titanium: a technical guide, Second edition, ASTM international, Ohio, 2000.

[33] V. Tuninetti, G. Gilles, V. Péron-Lührs, A.M. Habraken, Compression Test for Metal Characterization using Digital Image Correlation and Inverse Modeling, Procedia IUTAM 4 (2012a) 206-214.

[34] N.J. Hoff, Approximate analysis of structures in the presence of moderately large creep deformations, Quarterly of Applied Mathematics 12 (1954) 49–55.

[35] F. Pascon, 2D1/2 Thermal-Mechanical Model of Continuous Casting of Steel Using Finite Element Method. PhD thesis. Université de Liège, Liege, 2002.

[36] J. Nelder, R. Mead, A simplex method for function minimization, Computer Journal 7 (1965) 308-313.

[37] R. Hill, Constitutive dual potentials in classical plasticity, J. Mech. Phys. Solids 35 (1987) 23-33.

[38] N. Metropolis, A.W. Rosenbluth, M.N. Rosenbluth, A.H. Teller, E. Teller, Equation of state calculations by fast computing machines, J. Chem. Phys 21 (1953) 1087-1092.

[39] W.K. Hastings, Monte Carlo sampling methods using Markov chains and their applications, Biometrika 57 (1970) 97-109.

[40] X. K. Li, S. Cescotto, A mixed element method in gradient plasticity for pressure dependent materials and modelling of strain localization, Computer Methods in Applied Mechanics and Engineering 144 (1997) 287-305.

[41] A.M. Habraken, J.F. Charles, J. Wegria, S. Cescotto, Dynamic recrystallization during zinc rolling, Int. J. Forming Processes 1 (1998) 1292-7775.

[42] T. Belytschko, L.P. Bindeman, Assumed Strain Stabilization of the 4-Node Quadrilateral with 1-Point Quadrature for Nonlinear Problems, Computer Methods in Applied Mechanics and Engineering 88 (1991) 311-340.

[43] L. Duchêne, F. El Houdaigui, A.M. Habraken, Length changes and texture prediction during free end torsion test of copper bars with FEM and remeshing techniques, Int. J. Plasticity 23 (2007) 1417-1438.

[44] J.C. Simo, T.J.R. Hughes, On the variational foundations of assumed strain methods, J. Appl. Mech., ASME 53 (1986) 51-54.

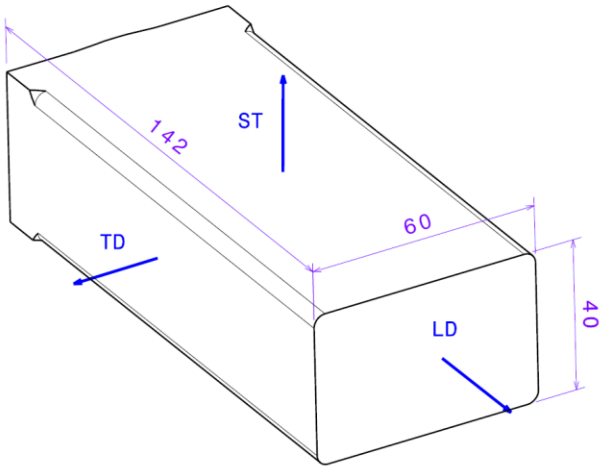

Figure 1. Material directions of the studied bulk piece of TA6V (dimensions in mm).

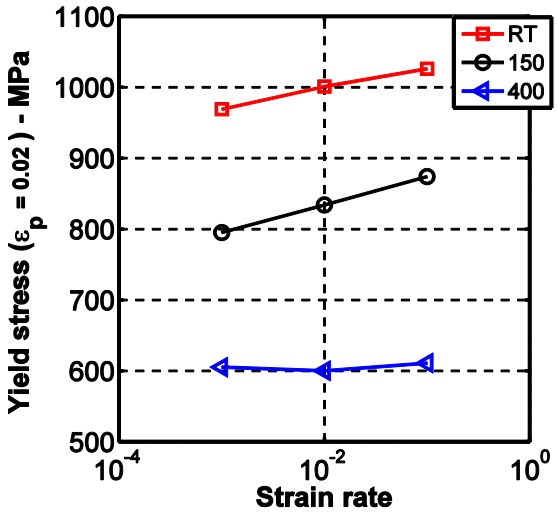

Figure 2. Yield stress in tension at 2% of plastic strain as a function of the strain rate at several temperatures.

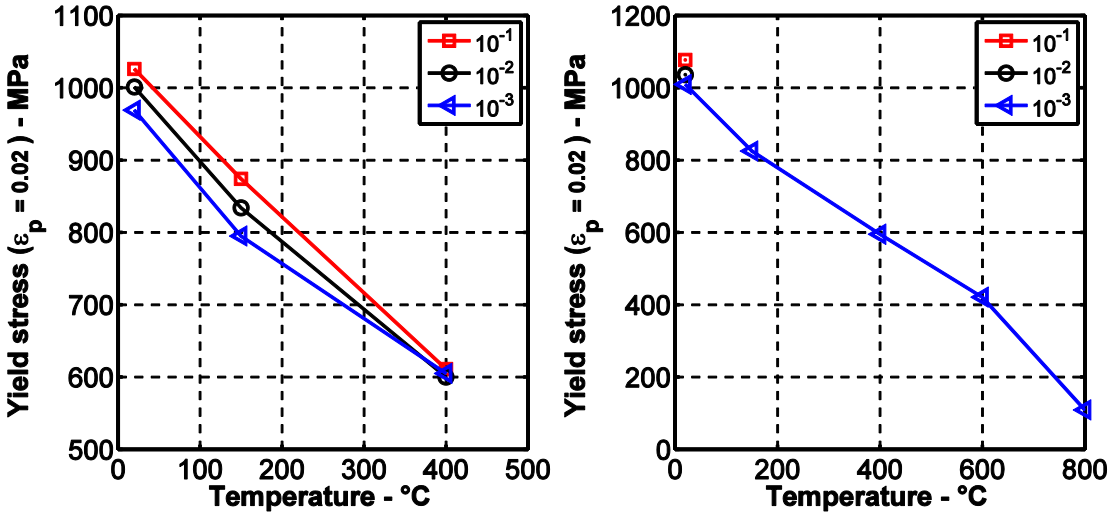

(a) **(b)**

Figure 3. Yield stress at 2% of plastic strain as a function of the temperature under several strain rates investigated. (a) Tension. (b) Compression.

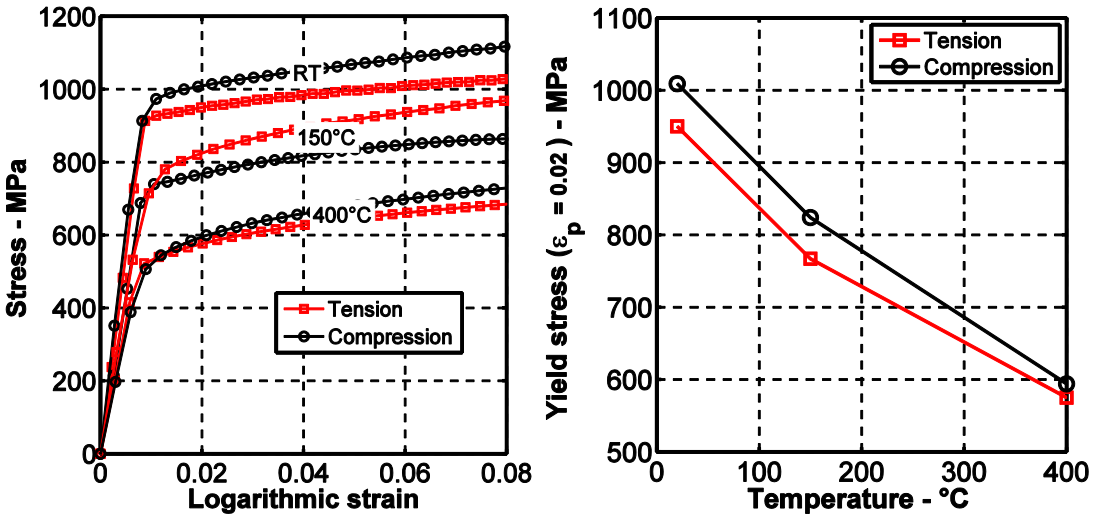

Figure 4. (a) True stress strain curves for monotonic tensile and compression in LD material direction at 10^{-3} s^{-1} and at RT, 150°C and 400°C (b) Yield stress in tension and compression at 2% of plastic strain as a function of the temperature.

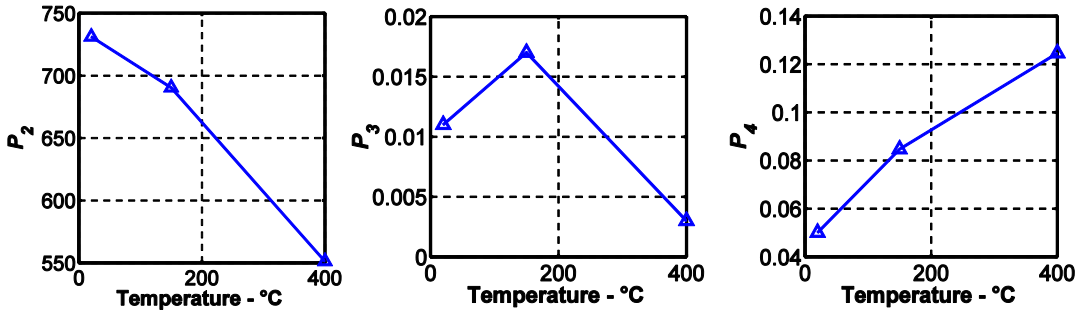

Figure 5. Variation of the NH parameters with the temperature. (a) P_2 related to strength, (b) P_3 related to strain rate sensitivity and (c) P_4 related to hardening.

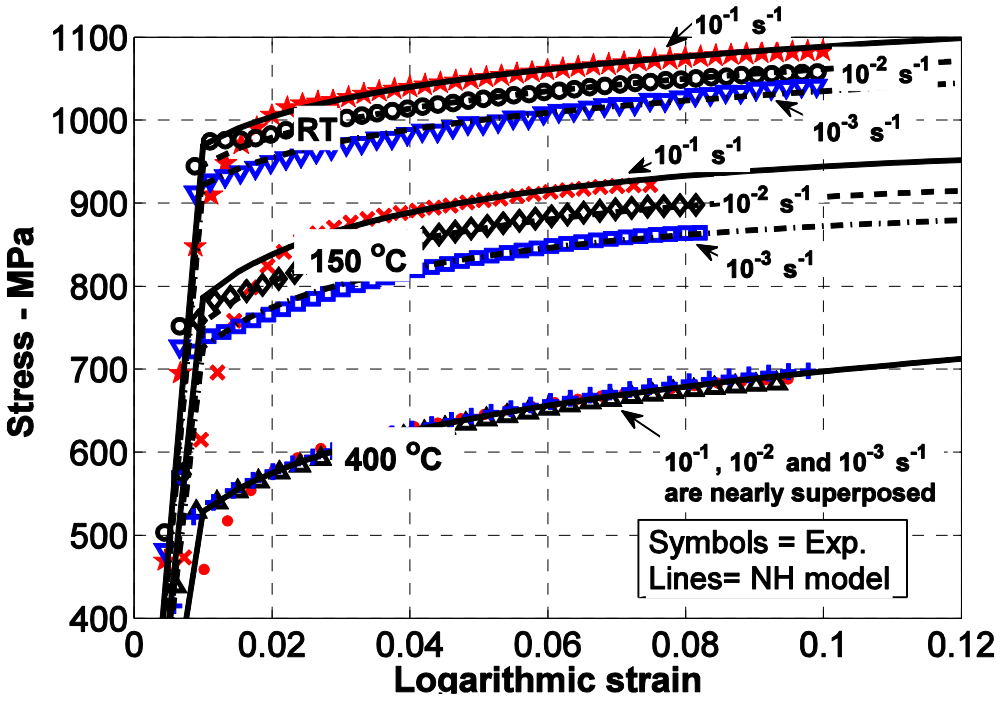

Figure 6. N–H law predictions of the true stress strain curves of tensile tests along with experimental data for RT, 150°C and 400°C at strain rates equal to 10^{-3}, 10^{-2} and 10^{-1} s^{-1}.

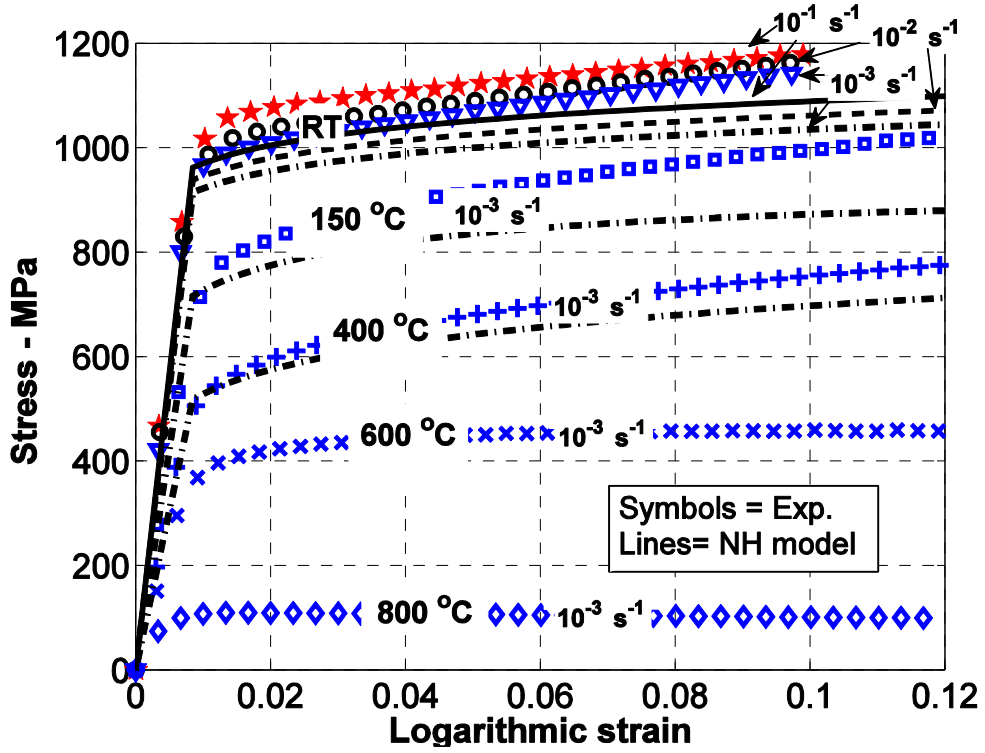

Figure 7. N–H law predictions of true stress strain curves of compression tests along with experimental data at strain rates equal to 10^{-3}, 10^{-2}, and 10^{-1} s^{-1} for RT, 150°C and 400°C.

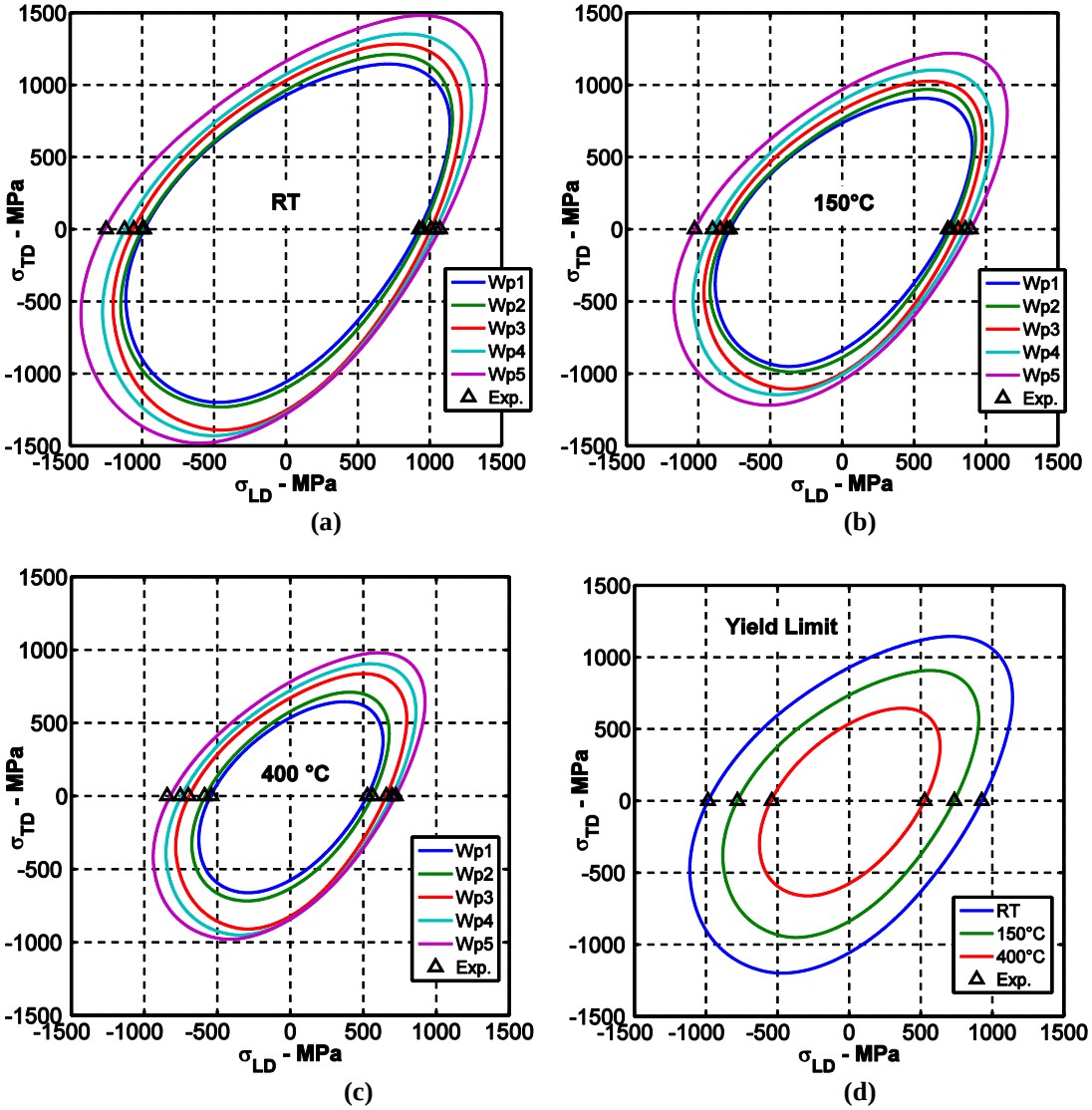

Figure 8. CPB06 yield surfaces for five *Wp* (a) at RT (Tuninetti et al. [29]), (b) at 150°C (c) at 400°C. (d) Initial CPB06 yield surfaces at RT, 150°C and 400°C.

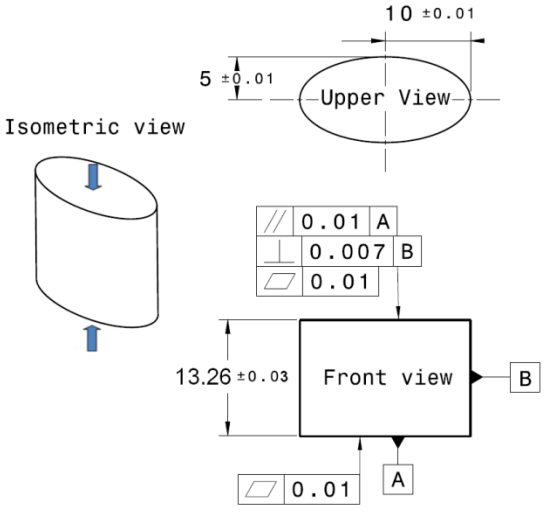

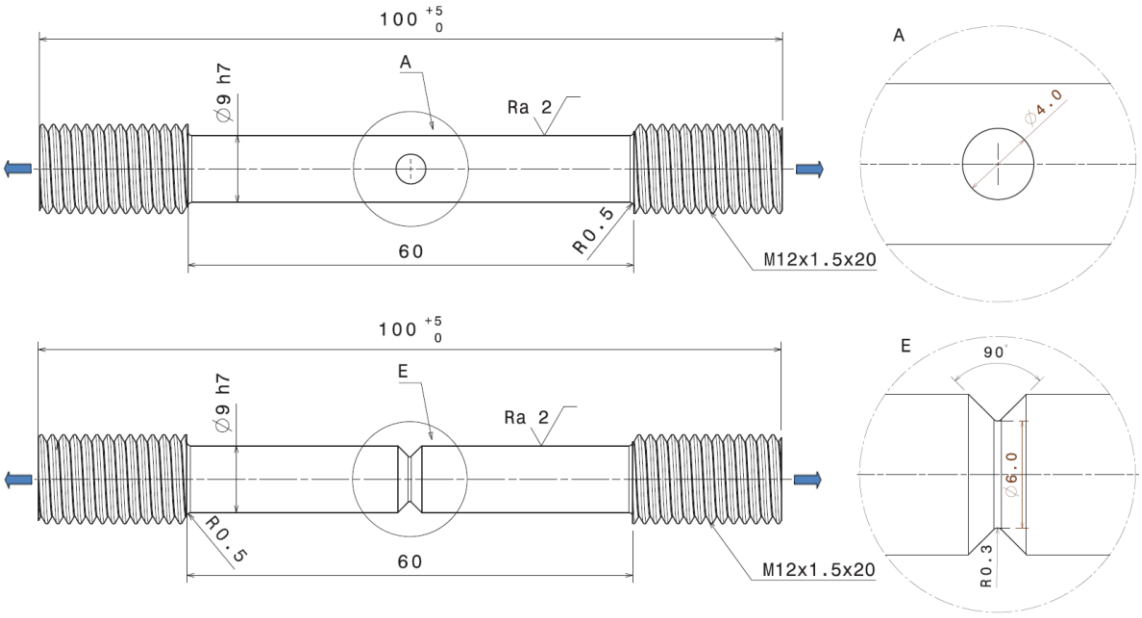

(b)

Figure 9. Geometries and dimensions of the specimens chosen for the evaluation of the models: (a) compression and (b) tensile specimens with axial load in LD direction.

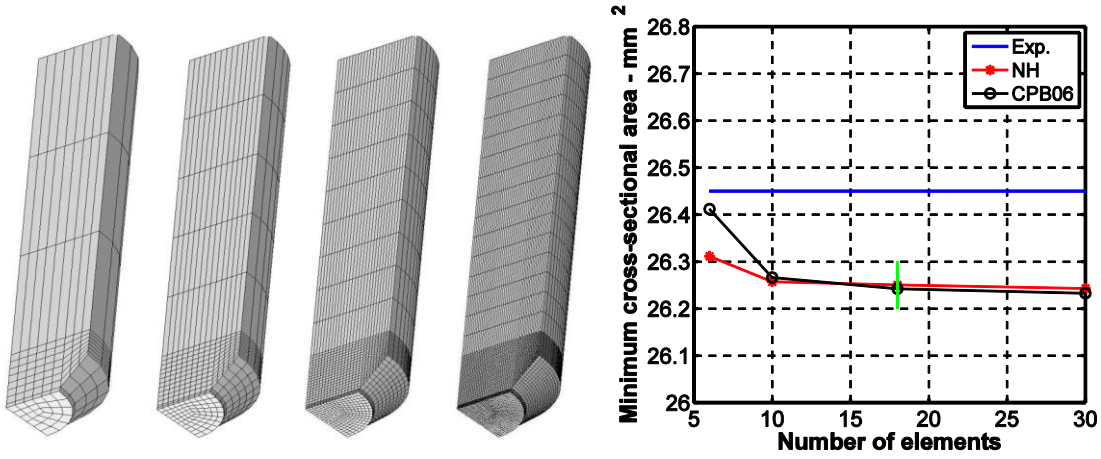

(a) **(b)**

Figure 10. Mesh sensitivity analysis. (a) V-notch round bars meshed with 6, 10, 18 and 30 elements along the radius (b) Evolution of the predicted minimum cross-sectional areas with the number of elements along the radio versus experimental result (experimental error equal to +-0.05 mm).

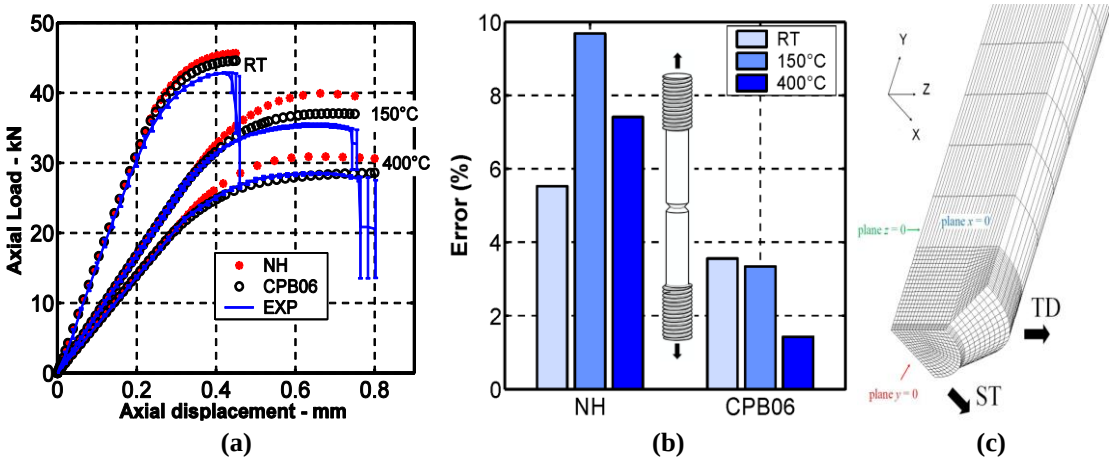

(a) (b) (c)

Figure 11. (a) Axial load predictions (LD direction) of the identified Norton-Hoff and CPB06 models applied to tensile tests on round bars with V-Notch. Experimental curves are shown with the error bar. (b) Percentage error on the load prediction. (c) Mesh of the one-eighth of the specimen.

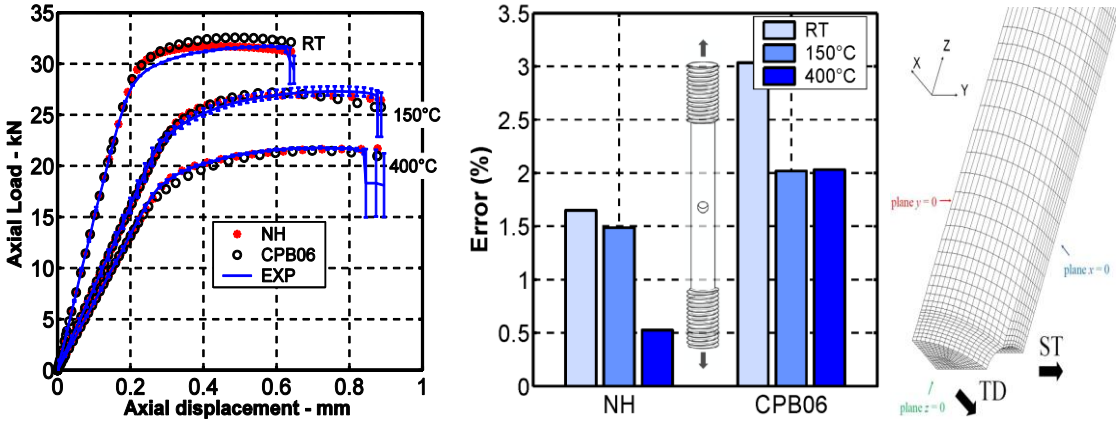

(a) (b) (c)

Figure 12. Axial (LD) Load predictions of the identified Norton-Hoff and CPB06 models applied to tensile tests on bars with a central hole. (b) Percentage error on the load prediction. (c) Mesh of the one-eighth of the specimen.

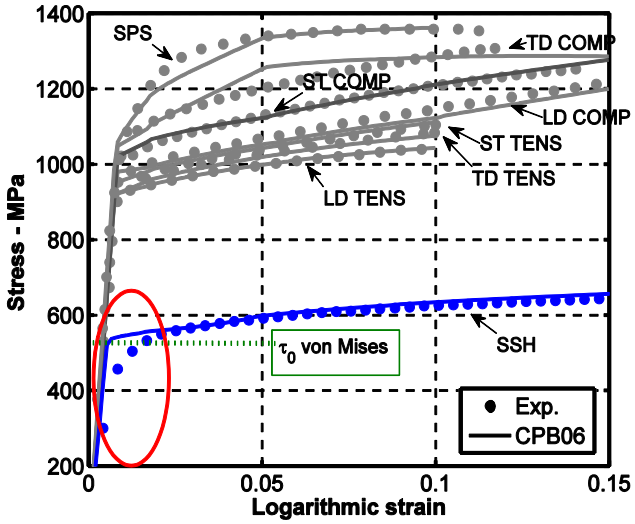

Figure 13. Experimental (Exp.) and CPB06 predictions of stress-strain curves in tension (TENS) and in compression (COMP) for the LD, TD and ST directions, plane strain LD-ST (SPS) and shear (SSH) LD-ST at RT (Tuninetti et al. [29]).

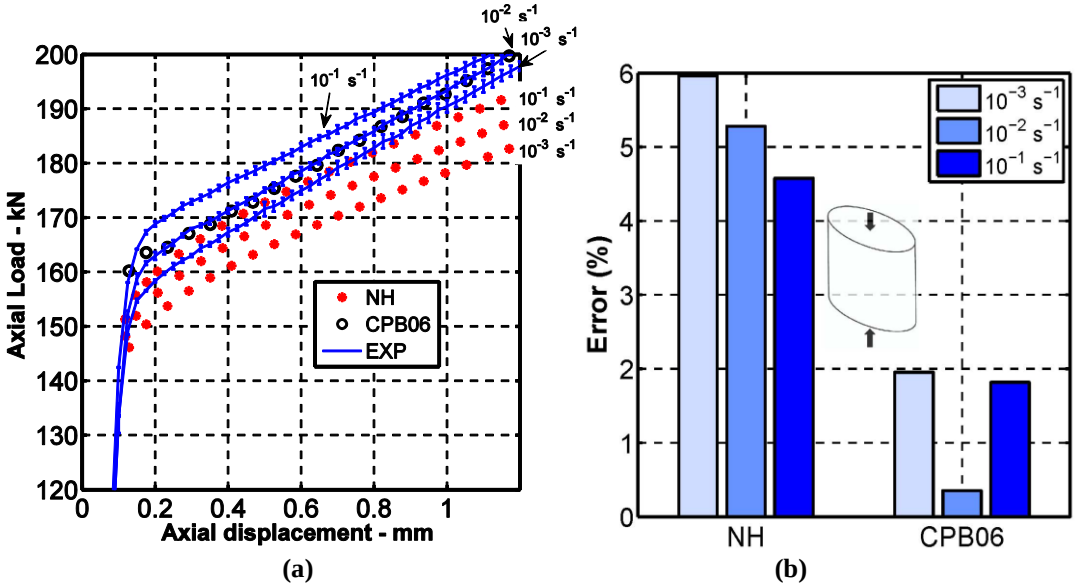

(a) **(b)**

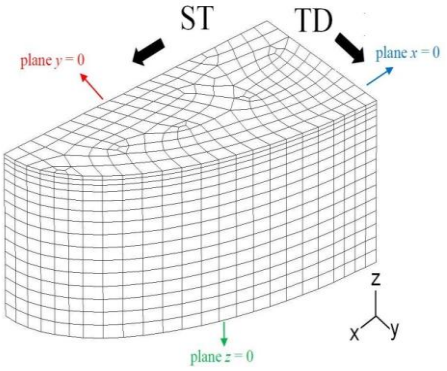

(c)

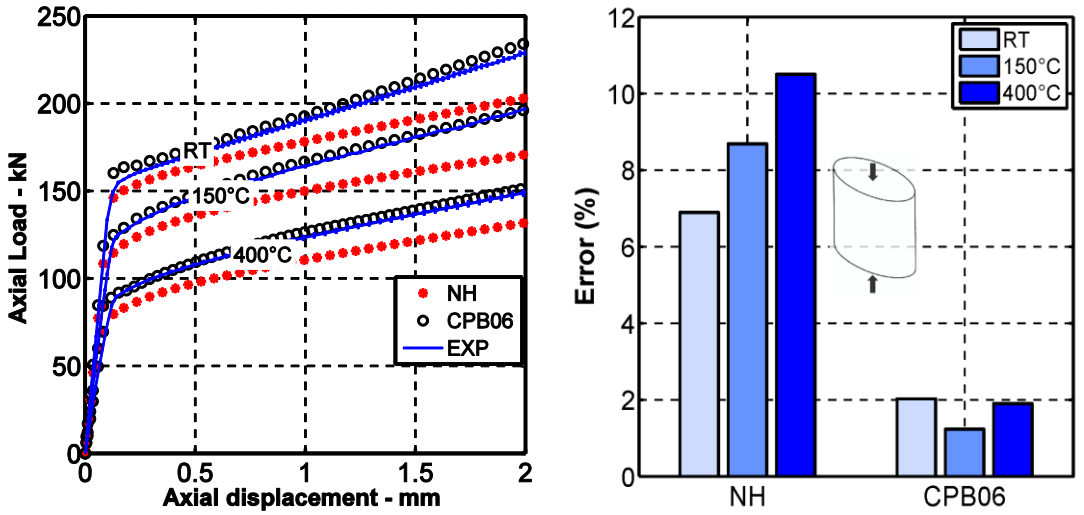

(d) **(e)**

Figure 14. Axial (LD) load predictions of the identified Norton-Hoff and CPB06 models applied to compression tests on elliptical cross-section. (a) Compression tests at RT and three strain rates equals to 10^{-3}, 10^{-2} and 10^{-1} s^{-1} (b) Percentage error on the load prediction associated with (a). (c) Mesh of one-eighth of the compression specimen. The initial height of the specimen is equal to 13.25 mm. (d) Compression tests at RT, 150°C and 400°C and at 10^{-3} s^{-1} (e) Percentage error on the load prediction associated with (d).

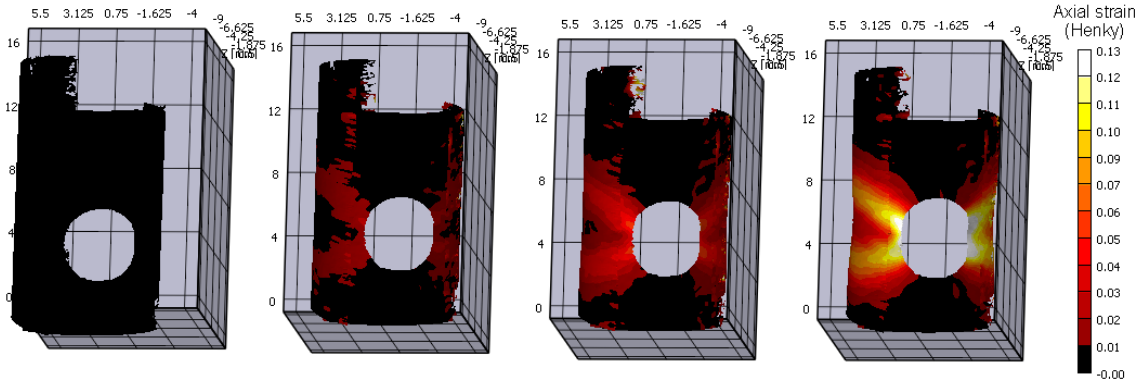

(a) **(b)** **(c)** **(d)**

Figure 15. Evolution of the true axial strain field and geometry of the specimen with central hole measured by 3D-DIC. (a) Initial measurements of the specimen without load, (b) at 0.2mm and (c) 0.4mm of axial displacement (gauge length=40mm), (d) state right before the fracture.

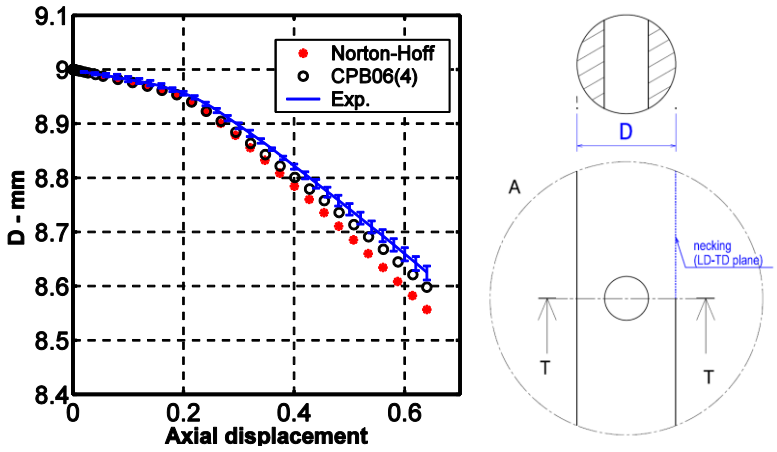

(a) (b)

Figure 16. (a) Comparison between DIC measurements, CPB06 and Norton-Hoff law predictions of the (b) diameter D of the cross-section of the central holed specimen.

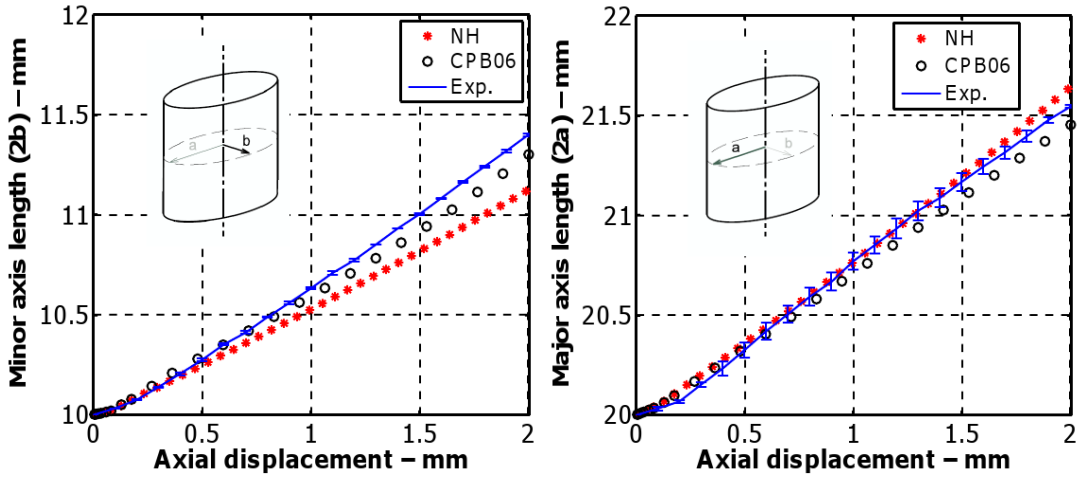

(a) (b)

Figure 17. Comparison between DIC measurements, CPB06 and Norton-Hoff law predictions of minor (a) and major (b) axis length of the elliptic cross-section of compression sample loaded in LD direction.

Al	V	Fe	N	O	C	Ti
6.1	4.0	0.3	0.05	0.20	0.08	Bal.

Table 1. Chemical composition of the TA6V alloy.

Test	Direction	Temperature °C	Strain rate s^{-1}	Young's Modulus *E* GPa ± Std. Dev.	Yield Strength σ_0 MPa (0.2% plastic strain) ± Std. Dev.
Tension	LD	RT	10^{-1}	-	-
			10^{-2}	113±1	973±1
			10^{-3}	111±1	927±3
		150	10^{-1}	63.5±4	743±5
			10^{-2}	74.9±3	784±1
			10^{-3}	85.7±5	740±4
		400	10^{-1}	57.6±6	451±3
			10^{-2}	68.0±1	531±2
			10^{-3}	70.8±2	528±2
Compression	LD	RT	10^{-1}	127±3	1013±5
			10^{-2}	125±4	986±4
			10^{-3}	122±1	968±3
		150	10^{-3}	74.3±4	772±5
		400	10^{-3}	66±7	540±4
		600	10^{-3}	41.6	386
		800	10^{-3}	11	106

Table 2. Experimental Young's modulus and yield stress for tension and compression at several temperatures and strain rates.

Temperature	P_1	P_2	P_3	P_4
RT	0	731.2	0.0110	0.0501
150	0	690.4	0.017	0.0847
400	0	551.2	0.003	0.1246

Table 3. Values of the identified parameters of the Norton-Hoff law for the TA6V alloy investigated at several temperatures.

	C_{11}	C_{12}	C_{13}	C_{22}	C_{23}	C_{33}	$C_{44}=C_{55}=C_{66}$
Surface 1	1	-2.373	-2.364	-1.838	1.196	-2.444	-3.607
Surface 2	1	-2.495	-2.928	-2.283	1.284	-2.446	4.015
Surface 3	1	-2.428	-2.920	1.652	-2.236	1.003	-3.996
Surface 4	1	-2.573	-2.875	1.388	-2.385	0.882	-3.926
Surface 5	1	-2.973	-2.927	0.534	-2.963	0.436	-3.883

Table 4. Anisotropy coefficients of CPB06 yield function (*a*=2) for TA6V for 5 plastic works levels defined in Table 5 (Tuninetti et al. [29]) identified at RT.

LD tension (ref. curve)	RT			150°C			400°C		
	A_0	B_0	C_0	A_0	B_0	C_0	A_0	B_0	C_0
	921	160	15.48	730	166	23.98	525	201	21.93
	W_p		k	W_p		k	W_p		k
Surface 1	1.857		-0.136	1.553		-0.136	1.364		-0.074
Surface 2	9.377		-0.136	7.682		-0.154	6.513		-0.089
Surface 3	48.66		-0.165	26.51		-0.150	40.78		-0.168
Surface 4	100.2		-0.164	28.14		-0.117	73.17		-0.148
Surface 5	206.6		-0.180	177.1		-0.153	146.8		-0.143

Table 5. SD coefficients *k* of CPB06 yield function for TA6V for 5 plastic works levels and for RT, 150°C and 400°C and material parameters of the reference curves (Tensile LD direction).